Influence of Turbulent Flow Field on Power Generation

Armin Hamta, Amir Hossein Birjandi, Eric L. Bibeau
Department of Mechanical and Manufacturing Engineering
University of Manitoba
Winnipeg, Manitoba
Email:hamtaa@cc.umanitoba.ca

***Abstract*—A 3D mapping technique is introduced to assist in finding optimal site locations for hydrokinetic turbines. The low and high turbulent statistics are mapped out in a open channel flow in which a cylinder is utilized as a source of disturbance. Measurements includes normal and Reynold's shear stresses, turbulent kinetic energy, and average velocity. Power coefficients for a vertical axis hydrokinetic turbine influenced under different wake regions of the cylinder are correspondingly mapped out and illustrated in a 3D matrix. Along with turbulent statistics and turbine performance, verification of the results and data collected are examined via the Frozen Taylor Hypothesis and the use of Taylor Macro-Scales.**

Keywords–Turbulent Statistics; Hydrokinetic Turbine; 3D Channel Mapping; Power Coefficient

I. Introduction

The industry of power generation has led to the development of many different methods of energy extraction from renewable and non-renewable energy sources. This aspect has become increasingly important given the limited fossil resources and climate change impacts. One such renewable resource which was adopted from the wind industry uses a turbine placed in the flow of a river or tide to generate hydrokinetic power [1], [2]. This is similar to how a wind turbine extracts the kinetic energy of the wind, although for a Hydrokinetic Turbine (HT) the energy density is nearly 800 times greater for the same flow velocity. This higher water density allows the extraction of energy at a lower velocity and area which is beneficial due to the complex nature of HT deployment [3], [4].

A. Hydrokinetic Turbine Performance

The percent of energy extracted from the flow is dependent on the efficiencies of mechanical and electrical components that are used to convert hydro kinetic energy into electrical energy. Once the turbine has been deployed the energy extraction becomes an independent process and no significant adjustments can be made to further increase the percent of energy extracted. As such there have been many attempts to increase the performance of its mechanical/electrical component by reducing the inefficiencies present, modifying the flow field, and optimize geometric configurations just to name a few. Specifically for the mechanical components, a few areas of focus for improvements have been on the geometry of the turbine blade, modifying the streamlines with a shroud enclosure, and the interaction of the river boundary layer with the turbine [3]. Flow statistics, including average velocity fields, are obtained in order to determine its correlation with the power curve to predict the performance of the turbine before deployment. This analysis typically undermines the influence of higher order turbulent flow statistics as the influence of the fluctuating component of the flow is deemed to negate itself due to the increase in kinetic energy available in the flow and the decrease in the turbine efficiency caused by the fluctuating component inducing greater fatigue and mechanical wear [5]. William D. Lubitz has shown in Ref [6] that the small Bergey XL.1 wind turbine (2.5 m blades, 1 kW) exhibited a 2% decrease in its power output within its operating range (4 m/s to 8 m/s) under turbulent intensities of less than 14%, and a 2% increase in power for turbulent intensities greater than 14%. The specific influence of turbulent flow patterns and its relationship with the power coefficient are analyzed for possibilities of taking advantage of regions in which there are increases in the normal power output of a given flow regime.

The total available power in the flow can be determined theoretically before the turbine is deployed based on the flow density ρ, cross-sectional area of the turbine A, and the average flow velocity V_{avg}.

$$P_{river} = \frac{1}{2}\rho A V_{avg}^3 \tag{1}$$

The amount of power harnessed from the turbine can be determined based on the torque measured from the turbine shaft T and the RPM of the blades. This technique was utilized using available transducers in the experimental setup.

$$P_{rotor} = T\frac{RPM * 2\pi}{60} \tag{2}$$

The power coefficient is defined as the ratio of the amount of power that is harnessed from the alternator P_{rotor} in relation to the amount of power theoretically available in the flow P_{river}. According to the Betz Limit, this value cannot exceed 59.3% due to the functional relationship derived for the possible power output of a flow reaching a maximum at an induction factor of 0.33.

$$C_p = \frac{2P}{\rho A V_{avg}^3} \tag{3}$$

Before a turbine is deployed at a site turbulent statistics of the location can be collected and analyzed in order to determine the power density of that region.

B. Turbulent Flow Field

The Reynold's number of a flow is used to classify a flow regime as turbulent or laminar; turbulent flow fields are characterized by their irregular flow conditions, random spatial and temporal variations, and non-linear governing equations. Given the environmental conditions of rivers, turbulent flow regimes are predominately present [7]. Turbulent flow can be divided into an average component and a fluctuating component according to Reynold's Decomposition [8],

$$U = \bar{U} + u' \tag{4}$$

where U is the instantaneous flow velocity, $\bar{U}$ is the average velocity, and u' is the fluctuating component.

The energy distribution of the fluctuating component is governed by the energy injected by the mean flow, cascading down the length scales from the large Taylor-Marco scales down to the small Kolmogorov scales, and finally the viscous dissipation, which converts the kinetic energy into thermal energy. The large length scales are determined by the physical scale of the flow domain while the small scales are set by the viscosity of the fluid and the dissipation rate. The turbulent kinetic energy (TKE) is a summation of the fluctuating components of the flow according to:

$$TKE = \frac{1}{2}[u'_x + u'_y + u'_z] \tag{5}$$

The amount of TKE in the flow can be determined by the use of transducers whose operating frequency exceeds the temporal frequency of the eddies present. Once the TKE is obtained it can be mapped along the channel; this provides a visual representation of the TKE flux along a flow path, around obstacles, and other regions of interest. This technique is utilized here in order to qualitatively observe the affect of disturbances in the flow and recovery of the flow's average velocity downstream.

In river flows disturbances occur as a result of natural obstacles such as debris, boulders, underwater structures and also from man-made structures. These wake fields have varying lengths, but as a general rule they last approximately 10 diameters away from the source [9]. Due to the site requirements of HT, multiple HTs will be located within close proximity of each other; like wind turbine farms. In this case the turbulent wake field of one HT will impact others downstream. By modeling how a HT is influenced by the wake field, optimal positioning can be established in order to ensure that the downstream turbines are not negatively affected. The usage of upstream anchors is another alternative investigated for manipulating the flow field in order to control the wake structures encountered by the HT [10].

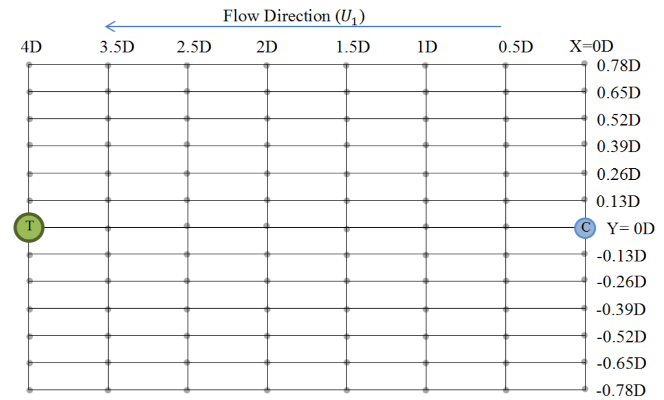

Fig. 1. Intersection points represented by dots are nodal points, based on the turbine diameter D, where the ADV was placed for turbulence measurements.

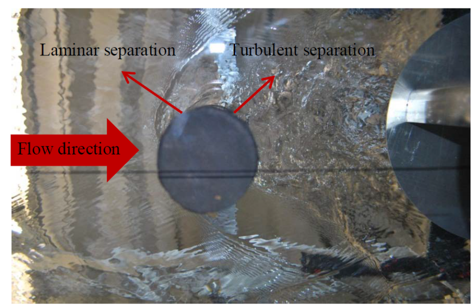

Fig. 2. Photo view of cylinder (on left) and turbine (on right) during close range testing [11]

II. Experimental Setup

A. Water Tunnel

The experiment was conducted at the University of Manitoba water tunnel. The experimental domain consisted of a 0.6 m by 0.6 m by 1.8 m test section with a 30 HP, 1800 RPM, 60 Hz variable frequency drive motor running the tunnel. The frequency driven motor, capable of providing 1.2 m/s average water velocity at a water level of 0.6 m, was set to a calibrated nominal value of 0.6 m/s for the experiments. A Nortek Vectrino AS Acoustic Doppler Velocimeter (ADV) set to 200 Hz was used to collect the low and high order turbulent statistics. A Rayleigh Torqsense transducer connected to the turbine's motor shaft collected corresponding data on the torque and RPM of the turbine. In order to simulate a turbulent flow regime caused by an obstruction, a 0.076 m diameter cylinder with 0.3 m height was placed upstream of the turbine. The cylinder is a representation of the disturbances that is found in river flows for the scaled turbine. The tunnel itself was divided up into nodal points based off the turbine diameter (D). Each nodal point is highlighted by a dark dot in Fig. 1 where the ADV was traversed in the first stage of the experiment.

Fig. 1 illustrates the coordinate layout of the final results presented in this paper; with the turbine located at the end of the channel in green and the cylinder located at the origin in blue. The flow is in the x-direction with the y-direction being used for lateral displacements of the ADV and cylinder along the channel. The number of nodal locations utilized for determining the turbine performance have fewer points due to turbine size limitations, although the general orientation of the results are as shown in Fig. 1.

B. Test Procedure

The methodology of energy extraction for this report, is not as important as the influence that the turbulent flow field has on the power output. This particular experiment involves the usage of a vertical axis squirrel cage 2 bladed hydrokinetic turbine with a diameter of 0.3 m and height of 0.3 m connected to a 0.25 HP motor. Turbulent flow fields are present in many alternate power generating units such as hydro-dams, and any steam driven turbine.

1) Turbulent Flow with Cylinder: In order to determine the wake region caused by the cylinder, the cylinder was fixed at coordinates (X = 0,Y = 0) with the tunnel operating at 0.6 m/s. The ADV was moved to each nodal points behind the cylinder in the absence of the turbine in order to establish the flow characteristics similarly to how field test are conducted in river sites [7]. Low and high order turbulent statistics were derived from the collected data and inserted into a matrix arranged with nodal points corresponding to points in the channel.

2) Clean Turbine Performance: In order to establish a baseline for the expected turbine performance, a control test was conducted with the turbine in the absence of the cylinder. The turbine was fixed at coordinates (X = 4,Y = 0) and the tunnel was operated under an average water speed of 0.6 m/s. This provided the power coefficient in the absence of an intentional turbulent source; this was later used to normalize the power coefficient obtained with the cylinder present. This comparison is important to distinguish which regions of the cylinder's wake produces positive and negative changes in the power output.

3) Turbulent Turbine Performance: In order to determine the turbine's performance in different parts of the wake region, the cylinder was moved sequentially to nodal points (based on turbine diameters) while the turbine was fixed at coordinates (X = 4,Y = 0). Torque and RPM data were collected and mapped along the test domain for each nodal point that the cylinder was moved to. The cylinder was traversed instead of the turbine due to the turbine's size limitations and the practicality of the experimental setup.

The setup also involved signal processing where the data obtained from the ADV was filtered for noise and unwanted spikes, as described next.

C. ADV Signal Filtering

The measured ADV data sets may contain Doppler noise due to aliasing of the return signal above the Nyquist frequency. This happens if the velocity of the flow velocity rises above or below the velocity range of the instrument [12], [13]. In addition to noise, the data set can contain large amplitude spikes, which are not simple to isolate. Entrained air bubbles are the main source of the spikes. Birjandi and Bibeau [12] conducted series of experiments in the University of Manitobas water-tunnel facility to assess the effects of air bubbles on the quality of the ADV velocity data set. They introduced a new hybrid method to remove spikes from the ADV velocity data set [14]. The advantage of this method over conventional methods is its accuracy in dealing with high spike density data sets, such as river velocity data sets. The ADV data set for the river flow data and the filtering algorithm code are available in Reference [14]. Before any further analysis on the laboratory turbulent velocity data set, the hybrid method is used to filter spikes.

D. Channel Geometry with Blockage Ratio

With the given geometry of the turbine and channel, the blockage ratio is a function of the projected area seen upstream/downstream of the flow and the RPM of the blades. The physical geometric blockage ratio fluctuates between the limits of where the turbine acts as a cylinder and does not let any water through (blockage of 25%), and the turbine being at a stand still where the minimum projected area is determined by the blade thickness (blockage of 0.83%). This is based on the equation

$$B = \frac{A_{turbine}}{A_{channel}} \tag{6}$$

where $A_{turbine}$ is the turbine projected area and $A_{channel}$ is the test domain cross-sectional area. As the RPM increases the blockage approaches, but never reaches, the maximum limiting value due to the increase in the fluid streamlines being diverted around the turbine. The lower limiting value is simply the position in which the turbine is stationary in which no power is generated. Due to the large variability of the blockage ratio and dependence on the power output, it was not taken into consideration and instead assumed that the turbine would be operating in similar conditions in site locations where multiple HT turbines would be deployed in parallel to each other and experience wall effects from neighboring turbines.

III. TURBULENT CHARACTERISTICS

The following graphs illustrate the flow statistics over the channel based of the nodal array construction. Note that the cylinder is located at (X = 0D, Y = 0D).

A. Verification

Several key observations can be obtained from the turbulent statistics which verifies the results based on known inputs and governing fluid flow equations. The average velocity of the flow as shown in Fig. 3 reaches the expected nominal 0.6 m/s value which the tunnel was set to. The normal shear stress qualitatively and quantitatively follow the governing TKE described by Eq. 5 where the sum of each term is equivalent to the TKE with a factor of $\frac{1}{2}$. These two points indicates that the results can be are valid for the experimental conditions in which they were performed.

It can be seen from the flow field's low and high turbulent statistics, the regions of the tunnel where there is an increase

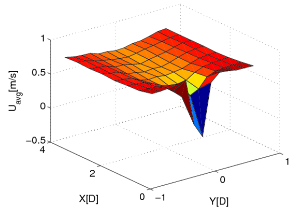

Fig. 3. Average Velocity

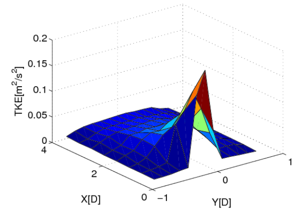

Fig. 4. TKE

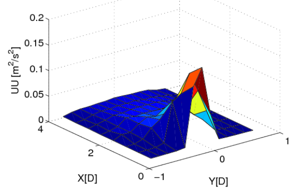

Fig. 5. Normal Stress UU

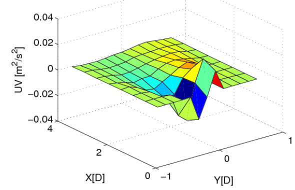

Fig. 6. Reynold's Stress UV

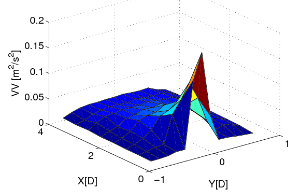

Fig. 7. Normal Stress VV

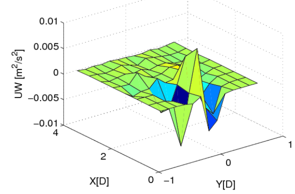

Fig. 8. Reynold's Stress UW

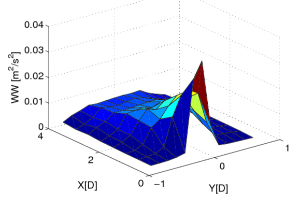

Fig. 9. Normal Stress WW

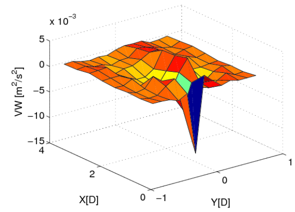

Fig. 10. Reynold's Stress VW

in the shear stress, TKE, and average velocity. The recovery of the flow field's TKE and average velocity takes approximately 2.5 turbine diameters. Besides the typical mean flow energy cascade, the sharp decrease in the TKE after the cylinder is a result of a lack of turbulent energy being introduced into the flow field as shown in Fig. 3, besides the typical mean flow energy cascade. The TKE recovers to the a normal state which can be seen developing in the far field downstream. The Reynold's shear stress fluctuations behind the cylinder indicate a flux in the transfer of momentum directly after the obstacle which also recovers after 2.5 turbine diameters. An interesting observation in the Reynold's Shear Stress UV, Fig. 6, is that the momentum transfer on the left of the cylinder is negative where as on the right side it is positive. This may be due to the slight mis-positioning of the cylinder in the channel which may have given preferential momentum transfer on one side more than another.

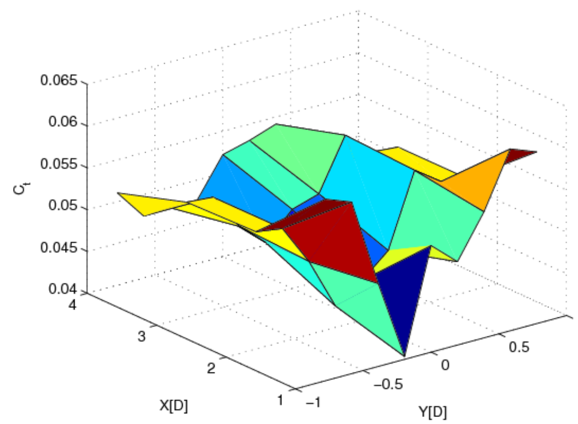

Fig. 11. Torque coefficient along channel

IV. Turbulent Influence on Turbine Performance

The RPM and torque data collected from the transducers at each nodal point that the cylinder was traversed to give a qualitative image of where the turbine's performance is influenced positively and negatively. The maximum turbine performance was taken at each nodal point which was approximately located at a tip speed ratio of 2.5. Fluctuations in the turbine performance were not considered for this experiment, instead only the maximum performance is evaluated in relation to the influence of the flow. The amount of torque illustrated in Fig. 11 can be determined from Eq. 7, where C_T is the torque coefficient of the turbine and R is the radius of the turbine.

$$T = \frac{1}{2}\rho C_T A R V_{river}^2 \tag{7}$$

The performance of the turbine with the influence of the cylinder was normalized by the results obtained from the control experiment in order to illustrate the change in turbine performance from the influence of the cylinder. Note that regions located directly after the cylinder on the left and right side have power coefficient that exceeds one. This is due to the slight increase in the water velocity due to the restriction that the cylinder causes. Based on the area next to the cylinder the normalized power coefficient can reach a max value of 1.22 which is just below the observed maximum, $C_p\ of\ 1.24$.

The positioning of HT in farms must be such that the wake region of one turbine does not negate the power output of downstream turbines. Based on the normalized power coefficient, as shown in Fig. 12, it is evident that the recovery of the flow field behind the cylinder is strong enough for the power coefficient to reach its control value within 3 turbine diameters. This translates into 11 cylinder diameters which agrees with the general rule that turbulent wake regions last approximately 10 (obstacle) diameters downstream of the turbulent source [9].

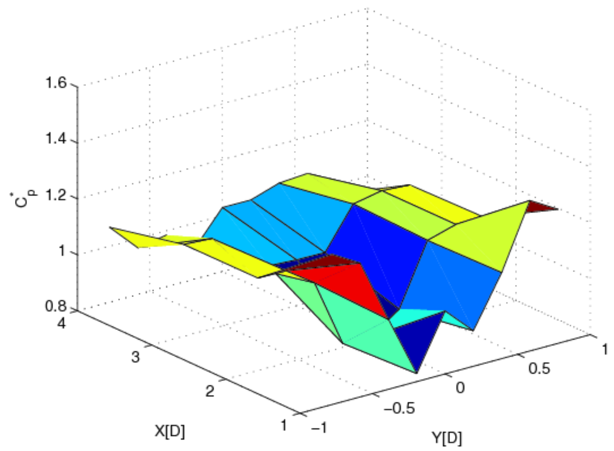

Fig. 12. Normalized Power Coefficient, with a recovery within 3 turbine diameters, equivalent to 11 cylinder diameters

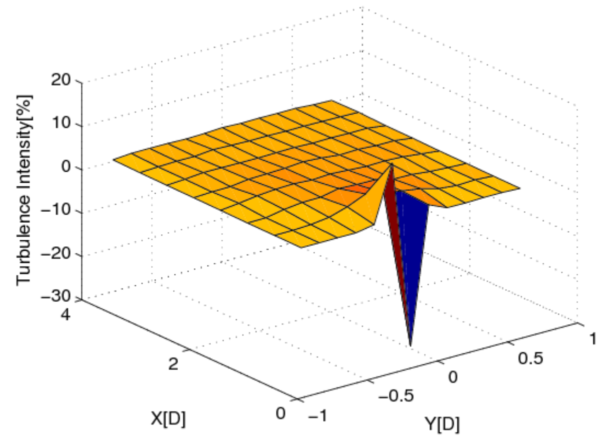

Fig. 13. Ratio of $I = U_{turb}/U_{avg}$ downstream of the cylinder, note the spikes directly behind the cylinder.

V. Experimental Validity

An additional component of the experiment can be investigated to confirm validity the data and results being illustrated. This involve the use of the Taylor Frozen Field Hypothesis to determine the length scales of the flow around the cylinder. The large Taylor Length Scale should be defined by the amount of space available for eddies to pass around the cylinder.

A. Taylor Frozen Field Hypothesis

The use of an ADV transducer with a high enough frequency allows the eddies of the flow regime to be captured before they pass by the sensors. The process of autocorrelation was utilized to determine the temporal scale between the data points, which was then translated to spatial scales through the relationship:

$$\langle \frac{d}{dt} \rangle = -u \langle \frac{d}{dx} \rangle \tag{8}$$

In order to translate the temporal data into a spatial reference frame, the Taylor Frozen Field Hypothesis must hold. This requires that the fluctuating component of the flow regime to be significantly smaller than the flow velocity [15]. In order to determine this ratio, local turbulence intensity (I), the fluctuating component of the flow was divided by the average flow velocity at each nodal point; a strict requirement that the intensity be less than 0.01 was set to fulfill the Taylor's Frozen Field Criteria. The two nodal points which are located directly behind the cylinder experience the greatest variations in the ratio due to the recirculation of the fluid and the near zero u_x velocity. In this case the order of the fluctuating component becomes comparable to the average velocity and causes the ratio to increase sharply. Exempting these extreme nodal points and with an average ratio along the field being 0.813, it is evident that Taylor's Hypothesis was not met. Although the criteria was not met, the use of the Taylor Frozen Field is still utilized in order to obtain the Taylor-Macro length scales as applied in similar experimental studies [16]. It is noted that discrepancies in the results of the length scales can be traced to the criteria not being fulfilled.

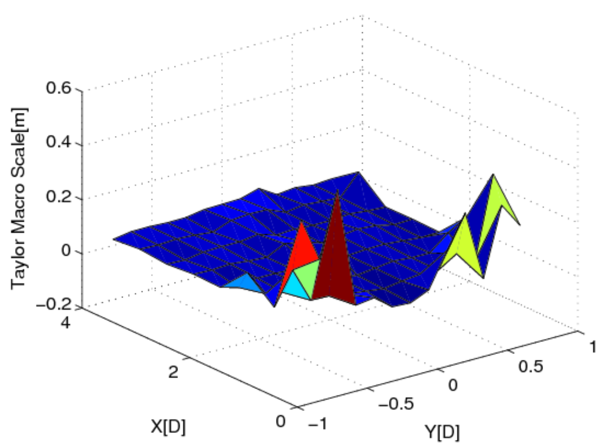

Fig. 14. Length scales directly adjacent to cylinder exhibit values less than physical space between channel wall and cylinder.

The Taylor Macro-Scale illustrated in Fig. 14 shows the average large length scale to be on the order of 0.04m, with the spiked regions omitted. The regions directly adjacent to the cylinder experience the influence of the obstacle have the largest length scales and disturbances. The average length scale in that region is 0.220 m which is lower the physical space beside the cylinder which is 0.262 m. This indicates that even with the strict Taylor Criteria failing the length scales do give reasonable results. It should be noted that the highest spike in the length scale is 0.4 m which may be a result of an upstream eddy which can have a maximum scale of 0.6 m based on the width of the channel.

VI. Conclusion

A quantitative mapping of the performance of a turbine in a water channel was illustrated with low and high order turbulent statistics. The flow regime's, normal and Reynold's shear stress, and TKE agreed with the expected flow patterns and illustrated that the influence of a cylinder as an obstacle reduces the power coefficient of a downstream turbine. The turbine's power coefficient recovery was at the expected distance of approximately 10 diameters away in relation to the obstacle. This methodology of 3D mapping of turbulent flow regimes when applied to river channel flow can be utilized for a qualitative and quantitative assessment of optimal regions where HT can be placed.

Acknowledgment

The authors would like to thank the NSERC/Manitoba Hydro Chair in Alternative Energy and NRCAN EcoII for funding.

References

[1] M. I. J. Q. M. Khan, G. Bhuyan, "Hydrokinetic energy conversion systems and assessment of horizontal and vertical axis turbines for river and tidal applications: A technology status review," 2009.

[2] M. S. Guney, "Evaluation and measures to increase performance coefficient of hydrokinetic turbines," *Elsevier Ltd*, 2011.

[3] S. Kassam, "The influence of atmospheric turbulence on the kinetic energy available during small wind turbine power performance testing," Master's thesis, University of Manitoba, Winnipeg, 2009.

[4] C. B. Craig Wessner, "Vertical axis hydrokinetic turbines: Practical and operating experience at pointe du bois, manitoba," 2002.

[5] B. C. Cochran, "Evaluation and measures to increase performance coefficient of hydrokinetic turbines."

[6] W. D. Lubitz.

[7] V. S. Neary, *Field Measurements at River and Tidal Current Sites for Hydrokinetic Energy Development: Best Practices Manual*, 2011.

[8] "Basics of turbulent flow." [Online]. Available: http://www.mit.edu/course/1/1.061/www/dream/SEVEN/SEVENTHEORY.PDF

[9] "Vectrino velocimeter manual," 2004.

[10] D. L. Gaden, "An investigation of river kinetic turbines:performance enhancements, turbine modelling techniques, and an assessment of turbulence models," Master's thesis, University of Manitoba, Winnipeg, 2007.

[11] A. H. Birjandi, "Effect of flow and fluid structures on the performance of vertical river hydrokinetic turbines," Ph.D. dissertation, Univ. of Manitoba, Winnipeg, 2012.

[12] E. B. Amir Birjandi, "Improvement of acoustic doppler velocimetry in bubbly flow measurements as applied to river characterization for kinetic turbines," *International Journal of Multiphase Flow*, 2011.

[13] E. L. B. Amir H. Birjandi, "Bubble effects on the acoustic doppler velocimeter (adv) measurements," *Proceedings of the ASME Fluids Engineering Division Summer Conference*.

[14] A. H. Birjandi, "River adv measurement and hybrid filter," 2010.

[15] W. J. Dahm and K. B. Southerland, "Experimental assessment of taylors hypothesis and its applicability to dissipation estimates in turbulent flows."

[16] N. V. Goring D., "Despiking acoustic doppler velocimeter data," *Journal of Hydraulic Engineering*.